Search for the alpha + He-6 decay of Be-10 via the O-16(O-18, Be-10*)Mg-24 reaction

Curtis, Neil; Ashwood, Nicholas; Freer, Martin; Munoz-Britton, T; Wheldon, Carl; Ziman, Victor; Brown, S; Catford, WN; Patterson, NP; Thomas, JS; Weisser, DC

DOI:
10.1088/0954-3899/36/1/015108

Document Version
Publisher's PDF, also known as Version of record

Citation for published version (Harvard):
Curtis, N, Ashwood, N, Freer, M, Munoz-Britton, T, Wheldon, C, Ziman, V, Brown, S, Catford, WN, Patterson, NP, Thomas, JS & Weisser, DC 2009, 'Search for the alpha + He-6 decay of Be-10 via the O-16(O-18, Be-10*)Mg-24 reaction', *Journal of Physics G: Nuclear and Particle Physics*, vol. 36, no. 1, pp. 015108. https://doi.org/10.1088/0954-3899/36/1/015108

J. Phys. G: Nucl. Part. Phys. **36** (2009) 015108 (12pp) doi:10.1088/0954-3899/36/1/015108

Search for the α + ^{6}He decay of ^{10}Be via the ^{16}O(^{18}O,^{10}Be*)^{24}Mg reaction

N Curtis[1], N I Ashwood[1], M Freer[1], T Munoz-Britton[1], C Wheldon[1], V A Ziman[1], S Brown[2], W N Catford[2], N P Patterson[2], J S Thomas[2] and D C Weisser[3]

[1] School of Physics and Astronomy, University of Birmingham, Edgbaston, Birmingham, B15 2TT, UK
[2] School of Electronics and Physical Sciences, University of Surrey, Guildford, Surrey, GU2 7XH, UK
[3] Department of Nuclear Physics, Research School of Physical Sciences and Engineering, Australian National University, Canberra, ACT 0200, Australia

Received 19 August 2008
Published 30 October 2008
Online at stacks.iop.org/JPhysG/36/015108

Abstract

A search for the α + ^{6}He decay of ^{10}Be has been performed using the $Li_2O(^{18}O,\alpha\,^{6}He)$ reaction at 80 and 100 MeV. An array of two Si–Si–CsI telescopes was used for the coincident detection of the breakup fragments. No evidence for the $^{16}O(^{18}O,\alpha\,^{6}He)^{24}$ Mg reaction was obtained, the cross-section being determined as $\sigma < 1.9$ μb and <3.9 μb at 80 and 100 MeV, respectively. The α + ^{15}N decay of ^{19}F was observed via the $^{7}Li(^{18}O,\alpha\,^{15}N)^{6}He$ reaction. For the ^{19}F excitation energy and centre-of-mass scattering angle ranges covered, the cross-sections are $\sigma = (31.7 \pm 6.6)$ μb at 80 MeV and (31.8 ± 6.6) μb at 100 MeV.

(Some figures in this article are in colour only in the electronic version)

1. Introduction

A considerable amount of experimental effort has been expended in recent years in an attempt to understand the structure of the neutron-rich nucleus ^{10}Be. Much of this work has been aimed at searching for the 4^+ member of the ground state rotational band, and in characterizing the nature of the proposed α:2n:α molecular band built on the α + ^{6}He cluster state at 6.18 MeV.

The 11.76 MeV state in ^{10}Be was first proposed as the 4^+ member of the ground state rotational band following a study of the $^{7}Li(\alpha, p)^{10}Be$ reaction [1]. This assignment was only tentative, however, as although the energy of the state was close to that predicted by the $J(J + 1)$ energy/spin systematics of the 0^+ ground state and 3.37 MeV 2^+ members of the band, the reproduction of the experimental angular distribution for the state with distorted wave Born approximation calculations was rather poor.

A study of the ^{7}Li(^{7}Li,α ^{6}He)α breakup reaction at 58 MeV [2] indicated the 11.76 MeV state to have $J^{\pi} = (4^{+}), 6^{+}$, suggesting it was unlikely to be a member of the ground state band. This assignment was, however, model dependent, as the ground state spin of the ^{7}Li beam and target in the entrance channel (3/2 + 3/2) had to be considered. In previous sequential breakup measurements spin determinations had only been obtained in reaction channels in which the beam, target and three final state particles all had ground state spin/parities of 0^{+}. In such a case the angular correlation at a centre-of-mass scattering angle $\theta^{*} = 0^{\circ}$ takes the form of a Legendre polynomial P_J, with J being the spin of the decaying resonant state (see for example [3]). In the ^{7}Li + ^{7}Li channel, however, the entrance channel spin had to be considered. The experimental angular correlation function at $\theta^{*} = 0^{\circ}$ was therefore fitted with a sum of associated Legendre polynomials, each weighted by a distribution chosen to reproduce the m-substate population. A Gaussian distribution, centred at $m = 0$, was used, leading to a model dependent assignment of $(4^{+}), 6^{+}$ for the 11.76 MeV state [2].

Most recently, Bohlen *et al* [4] have proposed a firmer assignment of 4^{+} for the 11.76 MeV state after studying the ^{12}C(^{12}C,^{14}O)^{10}Be two-proton pick up reaction at 211.4 MeV. This work again suggests the 11.76 MeV state is the 4^{+} member of the ground state band, although it is noted that the angular distribution shown has a somewhat limited range, and that the assignment does rely on a comparison to a coupled-channels (i.e. model dependent) calculation.

The ^{7}Li(^{7}Li,α ^{6}He)α breakup reaction was first studied by Soić *et al* [5] at 8 MeV. A new state was reported at an excitation energy (E_{x}) of 10.15 MeV in ^{10}Be, and a spin/parity of 4^{+} was proposed. This was based on the observation that the excitation energy was reasonably close to the 10.7 MeV expected from the rotational $J(J + 1)$ spacing of the 6.18 MeV 0^{+} and 7.54 MeV 2^{+} members of the α + ^{6}He cluster band. Two further studies of this channel, at 34 and 50.9 MeV [6], and at 58 MeV [2], both indicated an assignment of 3^{-} for the 10.15 MeV state. The same technique of fitting the experimental angular correlation function with a model dependent sum of m-substate weighted associated Legendre polynomials (see above) was used in both measurements. Recently, Freer *et al* [7] studied the 10.15 MeV state via a resonant elastic scattering measurement of the α(^{6}He,^{6}He)α reaction, using a radioactive ^{6}He beam and ^{4}He gas target. In this work the state was firmly assigned $J^{\pi} = 4^{+}$, importantly the assignment being made in a model independent way. The state was identified as the 4^{+} member of the α:2n:α molecular rotational band built upon the 0^{+} α + ^{6}He cluster state at 6.18 MeV. No assignment was made for the 11.76 MeV state in this work.

A summary of the current spin assignments for the α-decaying states in ^{10}Be, between the 7.4 MeV α-decay threshold and 20 MeV, is given in table 1 (all information not taken from [1, 2, 4–7] is from [8]). It is noted that above the 10.15 MeV state (firmly assigned 4^{+} in [7]) no definitive, model independent, spin information is available. The aim of this work was therefore to confirm the 4^{+} assignment to the 11.76 MeV state, to search for the 6^{+} members of both the ground state and α:2n:α molecular rotational bands, and to make assignments to as many other states in the region shown in table 1 as possible. In order to attempt this in a model independent way the experiment made use of the ^{16}O(^{18}O,α ^{6}He)^{24} Mg reaction. In this channel the beam, target and three final state particles all have ground state spin/parities of 0^{+}. This allows a model independent spin analysis to be performed (as noted above), by comparing the periodicity of the experimental angular correlation at $\theta^{*} = 0^{\circ}$ with Legendre polynomials of order J (where J is the spin of the decaying state). This reaction was chosen as the three-body decay Q-value, $Q_3 = -11.60$ MeV, is more favourable than that for the alternative ^{12}C(^{18}O,α ^{6}He)^{20}Ne channel, for which $Q_3 = -13.75$ MeV. The 11.76 MeV state in ^{10}Be is believed to be a member of the ground state rotational band and is therefore expected to have a very different structure to the α:2n:α molecular states. It is noted, however, that the

Table 1. The α-decaying states in ^{10}Be below 20 MeV.

E_x (MeV)	J^π	Reference
7.54	2^+	
9.56	2^+	
10.15	(4^+)	[5]
	3^-	[2]
	3^-	[6]
	4^+	[7]
10.57	$\geqslant 1$	
	3^-	[4]
	(3^+)	[4]
11.23		
11.76	(4^+)	[1]
	(4^+), 6^+	[2]
	4^+	[4]
(11.93)	(5^-)	
13.05		
13.80		
14.68		
17.79		

11.76 MeV state has been observed in previous studies of the α + ^{6}He decay of ^{10}Be [2, 6]. It was hoped, therefore, that the chosen reaction would populate the 11.76 MeV state in addition to the members of the α:2n:α molecular band.

2. Experimental details

The experiment was performed at the 14UD tandem Van de Graaff accelerator facility of the Australian National University. Beams of 80 and 100 MeV ^{18}O were used to bombard a 200 μg cm^{-2} lithium oxide (Li_2O) foil supported by a 10 μg cm^{-2} ^{12}C backing. The integrated beam exposure at 80 and 100 MeV was 2.9 and 0.93 mC, respectively.

The decay fragments were detected in coincidence in two detector telescopes. These were placed in-plane on opposite sides of the beam with centres located at 20.2° from the beam axis. Each consisted of three separate (50 × 50) mm elements. The first, a 70 μm thick double sided silicon strip detector, was segmented into 32 independent 3 mm wide strips, the 16 strips on the front face being horizontal and the 16 strips on the back face vertical. The second stage was comprised of a 500 μm thick resistive silicon strip detector (RSD) segmented into 16 separate, position sensitive strips. These provided position information with a resolution of ∼0.3 mm (in-plane) and ±1.5 mm (out-of-plane). The target to RSD distance was 124 mm. The third element in each telescope, a 10 mm thick CsI scintillator, was used to stop any highly energetic particles that passed completely through both silicon detectors. Together the three elements provided $\Delta E - E$ particle identification information for all isotopes from H to Li. The detectors were calibrated using a combination of α-particles from a 3-line α-source and 25 MeV ^{12}C ions elastically scattered from a ^{197} Au target. The energy resolution was ∼120 keV (FWHM) for the silicon detectors and ∼1.5% (FWHM) for the CsI crystals. As the inner edges of the detectors provided coverage to 8.8° from the beam axis, a mylar absorber was placed in front of each telescope after the calibration data had been taken. These absorbers, measured to be (181 ± 2) μm thick, were used to stop elastically scattered ^{18}O beam particles

from entering the ΔE detectors, reducing the counting and event pile-up rates. The lower mass and charge of the α and ^{6}He fragments of interest meant that these particles could pass through the mylar and enter the detector telescopes.

3. Analysis and results

Following the selection of events in which an α-particle and a ^{6}He nucleus were detected, the energies of the fragments were corrected to compensate for that lost in passing through the mylar absorbers. This correction varied from 9.3 to 3.0 MeV for the detected range of α-particle energies, 10–71 MeV. For the ^{6}He nuclei, detected over the range 11–42 MeV, the correction varied from 11.4 to 5.3 MeV. The total energy ($E_{\rm tot}$) in the exit channel was then calculated from $E_{\rm tot} = E_1 + E_2 + E_{\rm rec} = E_{\rm beam} + Q_3$. Here E_1 and E_2 correspond to the energies of the two detected particles following the correction for the energy lost in the mylar, $E_{\rm beam}$ the beam energy and Q_3 the three-body Q-value for the reaction. The recoil energy, $E_{\rm rec}$, was determined by applying momentum conservation between the beam and the two detected particles and by making an assumption of the recoil mass. All reactions were assumed to occur at the centre of the 200 μg cm^{-2} Li_2O target. The beam energy was therefore corrected for the calculated energy loss in half of this thickness, $\Delta E = 410$ keV at 80 MeV and 350 keV at 100 MeV. As the calculated α-particle and ^{6}He energy loss in the target was only 10–40 keV over the range of detected energies, a target energy loss correction was not applied to these particles.

In figures 1(a)–(c) the $E_{\rm tot}$ spectra for the 80 MeV beam data are shown. In figure 1(a) the data have been reconstructed assuming the reactions occurred from the ^{16}O content of the target. The Q-value for the ^{16}O(^{18}O,α ^{6}He)^{24} Mg reaction is $Q_3 = -11.60$ MeV. The arrow labelled $Q_{\rm ggg}$ indicates the predicted position for events in which all three final state particles were emitted in their ground states, $E_{\rm beam} + Q_3 = 67.99$ MeV. Although a peak is observed at approximately this energy, (67.15 $\pm$ 0.03) MeV, it has a large width of $\approx$2700 keV. The background events, which extend to $E_{\rm tot}$ values greater than the beam energy, are most likely to arise from pile-up events in which the detected α-particle and ^{6}He are uncorrelated. In figure 1(b) the same data have been reconstructed assuming the ^{7}Li(^{18}O,α ^{6}He)^{15}N reaction ($Q_3 = -5.99$ MeV). A prominent peak is seen at an energy of (73.46 $\pm$ 0.01) MeV in good agreement with the predicted $Q_{\rm ggg}$ peak position for this channel (73.60 MeV). The width of this peak, (790 $\pm$ 15) keV, is considerably narrower than that observed in figure 1(a). A much weaker peak may also be seen in figure 1(b) at (68.12 $\pm$ 0.03) MeV with a width of (590 $\pm$ 80) keV. This energy is again in good agreement with the predicted position of events in which the ^{15}N was produced in either the first or second excited state (5.27 and 5.30 MeV, respectively). The average predicted $E_{\rm tot}$ for these two excited states is 68.31 MeV, indicated by the arrow labelled $Q_{\rm ggg12}$. In figure 1(c) the data are shown reconstructed assuming the reactions occurred from the ^{12}C backing of the target. A very broad peak, FWHM $\approx$ 2000 keV, is seen at (69.25 $\pm$ 0.02) MeV. The predicted $Q_{\rm ggg}$ peak energy for the ^{12}C(^{18}O,α ^{6}He)^{20}Ne reaction ($Q_3 = -13.75$ MeV) is 65.84 MeV (indicated by the arrow). Although there is some suggestion of a peak at this energy it is broad and very weak. The broad peaks at (67.15 $\pm$ 0.03) MeV in figure 1(a) and at (69.25 $\pm$ 0.02) MeV in figure 1(c) correspond to the same events as those in the narrow peak at (73.46 $\pm$ 0.01) MeV in figure 1(b). It seems clear, therefore, that the detected α + ^{6}He events in the 80 MeV beam data arose primarily from the ^{7}Li content of the target via the ^{7}Li(^{18}O,α ^{6}He)^{15}N reaction. When these events are reconstructed with an incorrect recoil mass in the $E_{\rm tot}$ calculation the $Q_{\rm ggg}$ peak is significantly widened, producing the broad peaks seen in figures 1(a) and (c).

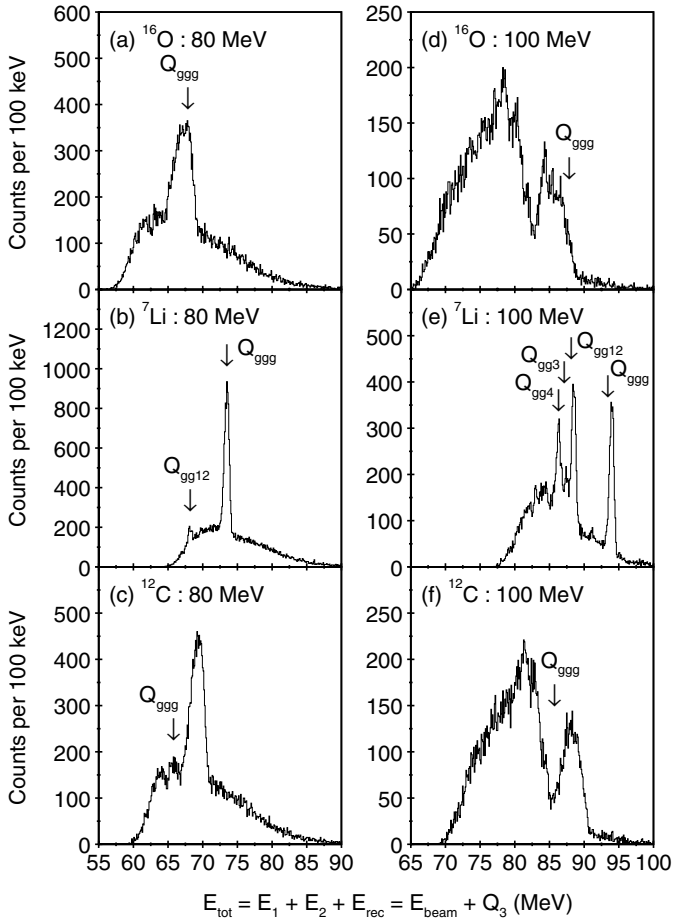

Figure 1. Total energy spectra at 80 and 100 MeV assuming breakup from the (a) and (d) ^{16}O, (b) and (e) ^{7}Li and (c) and (f) ^{12}C content of the target. The arrows indicate the predicted energies of the Q-value peaks (see text).

The $E_{\rm tot}$ spectra for the 100 MeV beam data are shown in figures 1(d)–(f). In figure 1(d) the data have been reconstructed assuming an ^{16}O target. The predicted $Q_{\rm ggg}$ peak position, 88.05 MeV, is indicated by the vertical arrow. There is no evidence for a peak at this energy. In figure 1(e) the data are shown reconstructed assuming the reactions occurred from the ^{7}Li content of the target. A strong peak is observed at (93.96 ± 0.01) MeV with a width of (730 ± 15) keV. This is reasonably close to the predicted $Q_{\rm ggg}$ peak energy of 93.66 MeV. A second peak, labelled $Q_{\rm gg12}$, is observed at $E_{\rm tot} = (88.50 \pm 0.01)$ MeV with a width of (700 ±30) keV. This corresponds to events in which the ^{15}N was produced in either the first (5.27 MeV) or second (5.30 MeV) excited state, for which the predicted average $E_{\rm tot}$ is 88.37 MeV. Two additional peaks, labelled $Q_{\rm gg3}$ and $Q_{\rm gg4}$, appear at energies of (87.47 ± 0.03) and (86.34 ± 0.02) MeV, with widths of (715 ± 105) and (815 ± 75) keV, respectively. These correspond to events in which the ^{15}N was produced in the 6.32 MeV third and 7.16 MeV fourth excited states. For these decays $E_{\rm tot}$ is predicted to be 87.33 and 86.50 MeV, respectively. In figure 1(f) the data are shown reconstructed assuming a ^{12}C target. There is no evidence for a peak at the

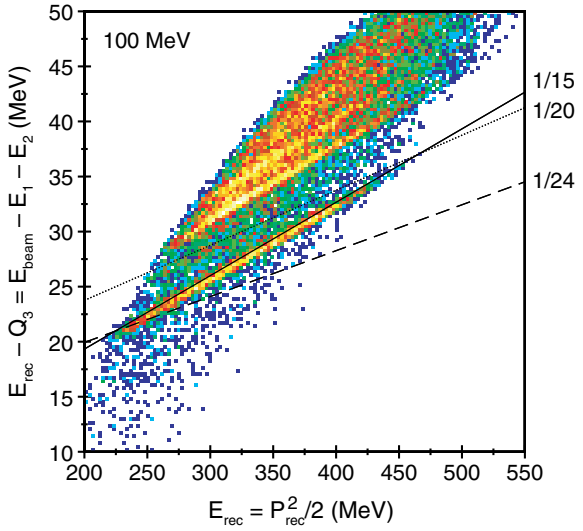

Figure 2. Plot of $E_{\rm rec} - Q_3$ against $P^2_{\rm rec}/2$ for the $Li_2O(^{18}O,\alpha\,^6He)$ reaction at 100 MeV. The predicted $Q_{\rm ggg}$ loci with slopes of 1/15, 1/20 and 1/24 (1/recoil mass) are indicated by the various lines.

predicted $Q_{\rm ggg}$ peak energy of 85.90 MeV. As in the case of the 80 MeV beam data shown in figures 1(a)–(c), it is clear from figures 1(d)–(f) that the α + ^{6}He coincidences seen in the 100 MeV beam data set arose from the ^{7}Li content of the target. The broad structures appearing at ∼78 and ∼86 MeV in figure 1(d) and at ∼81.5 and ∼88.5 MeV in figure 1(f) correspond to the $Q_{\rm ggg}$, $Q_{\rm gg12}$, $Q_{\rm gg3}$ and $Q_{\rm gg4}$ events observed in figure 1(e). As these have been reconstructed with an incorrect recoil mass the clear peaks seen in figure 1(e) merge to form the unresolved broad structures observed in figures 1(d) and (f).

The conclusion that the observed α + ^{6}He coincidences occurred via the ^{7}Li content of the target is supported by figure 2. This is essentially a spectrum of the recoil energy determined from energy conservation (plotted as $E_{\rm rec} - Q_3 = E_{\rm beam} - E_1 - E_2$) against that determined from momentum conservation (plotted as $\mathbf{P}^2_{\rm rec}/2$, where $\mathbf{P}_{\rm rec}$ is the recoil momentum). Because the recoil energy obtained from momentum conservation is plotted as $\mathbf{P}^2_{\rm rec}/2$ and not $\mathbf{P}^2_{\rm rec}/2m_{\rm rec}$ (where $m_{\rm rec}$ is the recoil mass), events corresponding to the $E_{\rm tot}$ $Q_{\rm ggg}$ peak will lie on a line with a slope of $1/m_{\rm rec}$ (with an intercept on the $E_{\rm rec} - Q_3$ axis equal to $-Q_3$). In figure 2 the predicted $Q_{\rm ggg}$ locus for the $^{16}O(^{18}O,\alpha\,^6He)^{24}$ Mg reaction ($1/m_{\rm rec} = 1/24$) is indicated by the dashed line, that for the $^{12}C(^{18}O,\alpha\,^6He)^{20}Ne$ channel ($1/m_{\rm rec} = 1/20$) by the dotted line and that for the $^7Li(^{18}O,\alpha\,^6He)^{15}N$ reaction ($1/m_{\rm rec} = 1/15$) by the solid line. Whilst there is no evidence for a locus of events under either the ^{16}O (dashed) or ^{12}C (dotted) lines, a clear locus is seen under the ^{7}Li (solid) line. Placing a software window around these events therefore allows the $^7Li(^{18}O,\alpha\,^6He)^{15}N$ $Q_{\rm ggg}$ channel to be selected. The two clear loci of events, parallel to the solid line, appearing at higher values of $E_{\rm rec} - Q_3$, correspond to the $Q_{\rm gg12}$ and $Q_{\rm gg4}$ peaks seen in figure 1(e). The $Q_{\rm gg3}$ peak in figure 1(e) is very weakly populated and hence does not show up clearly in figure 2. The spectrum shown in figure 2 was obtained from the 100 MeV beam data set. The 80 MeV beam spectrum is essentially the same and is not shown.

Following the selection of the $^7Li(^{18}O,\alpha\,^6He)^{15}N$ $Q_{\rm ggg}$ events, the excitation energies in ^{10}Be and ^{19}F were reconstructed. For binary breakup the decay energy ($E_{\rm decay}$) for a decaying

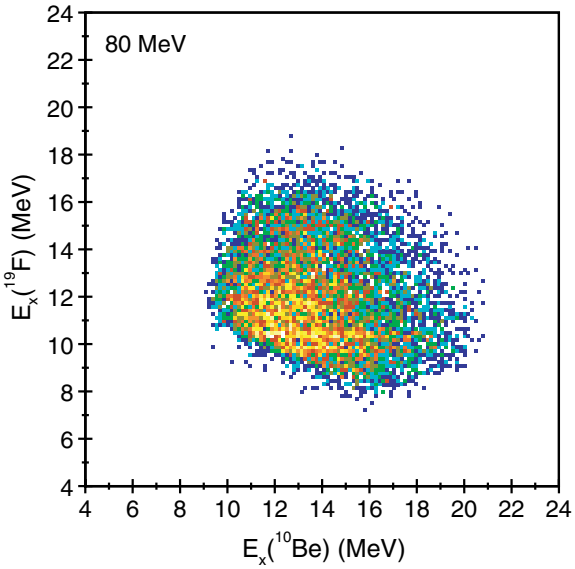

Figure 3. Excitation energy in ^{10}Be against excitation energy in ^{19}F for the 80 MeV beam data.

parent nucleus may be obtained from the kinetic energies and momenta of the decay fragments: $\mathbf{P}_{\text{Parent}} = \mathbf{P}_1 + \mathbf{P}_2$, $E_{\text{Parent}} = \mathbf{P}^2_{\text{Parent}}/2m$ (where m is the mass of the parent nucleus) and $E_{\text{decay}} = E_1 + E_2 - E_{\text{Parent}}$. The decay energy is related to the excitation energy of the decaying parent nucleus via $E_{\text{x}} = E_{\text{decay}} - Q_2$, where Q_2 is the 2-body decay Q-value. The excitation energy in ^{10}Be was therefore obtained from the decay energy of the detected α and ^{6}He fragments. The ^{19}F excitation energy was obtained from the decay energy of the detected α-particle and the reconstructed recoiling ^{15}N. These are shown plotted in figure 3 (for the 80 MeV beam data). The corresponding spectrum for the 100 MeV beam data is similar and is not shown. In figure 3 any excited states populated in ^{10}Be and ^{19}F would appear as vertical and horizontal loci, respectively. Any states populated in the ^{6}He + ^{15}N decay of ^{21}F, the third combination of final state particles, would appear as diagonal loci with negative slope. There is no evidence for either vertical or diagonal loci in the spectrum, whereas horizontal loci, corresponding to the α + ^{15}N decay of ^{19}F, may just be seen close to $E_{\text{x}}(^{19}\text{F}) = 10$ MeV.

The ^{10}Be excitation energy spectra, reconstructed from the detected α and ^{6}He fragments, are shown in figure 4. There is no real evidence for peaks indicating the population of states in ^{10}Be in either the 80 or 100 MeV beam data (figures 4(a) and (b), respectively), and in particular there is no convincing evidence for the 11.76 MeV state of interest. The excitation energy spectra for ^{19}F, obtained from the detected α-particle and the reconstructed recoiling ^{15}N, are shown in figure 5. The dashed lines indicate the predicted detection efficiencies obtained from a Monte Carlo simulation. In the Monte Carlo code the initial ^{7}Li(^{18}O,^{19}F)^{6}He two-body reaction was simulated using a random number generator that mimicked the experimentally measured centre-of-mass scattering angle (θ*) distribution. An isotropic distribution was used to simulate the sequential decay of ^{19}F into the α and ^{15}N fragments. The predicted detection efficiencies, shown in figure 5 by the dashed lines, were obtained from the number of Monte Carlo events in which both fragments were found to be within the angular ranges covered by the telescopes, and above the low energy thresholds arising from the performance of the detectors and the mylar absorbers. In order to determine the experimental resolution the energies and

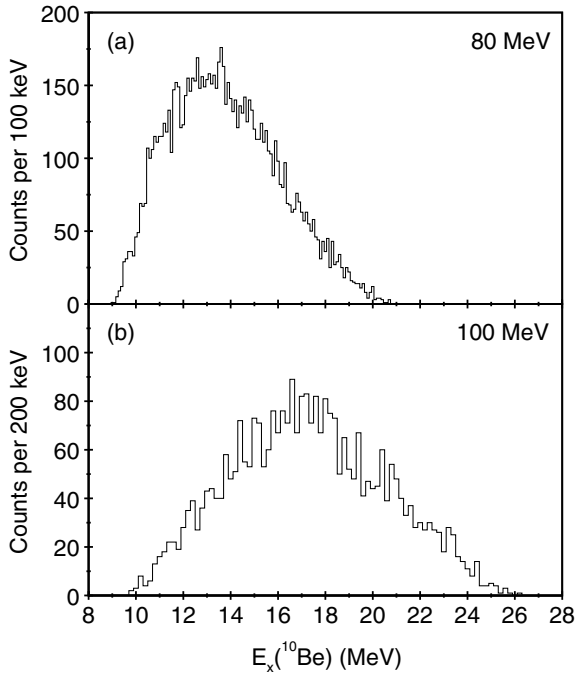

Figure 4. Excitation energy in ^{10}Be for the (a) 80 and (b) 100 MeV beam data.

angles of the particles were smeared from those values calculated by the kinematics section of the code. This allowed various physical effects to be simulated. These include the energy loss of the beam and fragments in the target, the energy and angular straggling of the fragments in the target, and the energy and position resolution of the detector telescopes. The smeared pseudo-data generated by the code were then reconstructed in the same manner as the real data, allowing the width of the peaks observed in the excitation energy spectra to be predicted. Two distinct peaks are observed in the 80 MeV beam data set, shown in figure 5(a), at 9.72 and 10.32 MeV. The same peaks also seem to be populated in the 100 MeV beam data (figure 5(b)), appearing at (9.82) and (10.41) MeV, along with additional peaks at (7.98), (8.98), (11.56) and (15.18) MeV. These are listed in table 2, as are the widths of the three most prominent peaks. These were obtained, for the 10.32 MeV peak in the 80 MeV beam data and for the 15.18 MeV peak in the 100 MeV beam data, from the quadrature subtraction of the predicted experimental resolution from the observed width. In the case of the 9.72 MeV peak in the 80 MeV beam data (figure 5(a)), the observed width of (255 $\pm$ 43) keV is identical to that predicted by the Monte Carlo, suggesting the natural width is very narrow. Hence only an upper limit to the width can be given in table 2. The approximate range over which peaks are observed in figure 5 is 7–17 MeV. In this region there are over 130 known states in ^{19}F [9], and as such it is not possible to identify which of the known states the peaks observed in figure 5 correspond to. The one exception may be the peak observed at 15.18 MeV in figure 5(b), which might be associated with the 14.72 or 14.74 MeV states, previously observed in the ^{18}O(p,α)^{15}N reaction [9]. The energy shift of 450 keV is somewhat greater than the usual 200–300 keV systematic uncertainty in E_x typical in breakup measurements, however, although no other α-decaying states are known in this region. The excitation energy spectra for the α + ^{15}N*

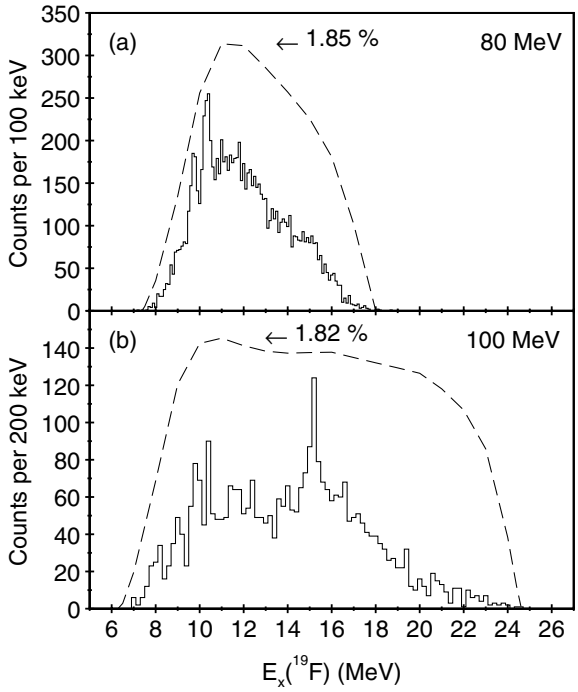

Figure 5. Excitation energy in ^{19}F for the (a) 80 and (b) 100 MeV beam data. The dashed lines indicate the predicted detection efficiencies, for which the peak values are given (see text).

Table 2. Peaks observed in the α + ^{15}N decay of ^{19}F.

E_x (MeV)	FWHM (keV)	Beam energy (MeV)
9.72 ± 0.02	<255	80
10.32 ± 0.02	150 ± 40	80
(7.98 ± 0.06)		100
(8.98 ± 0.05)		100
(9.82 ± 0.03)		100
(10.41 ± 0.04)		100
(11.56 ± 0.09)		100
15.18 ± 0.03	325 ± 85	100

decay of ^{19}F, obtained by selecting events in the Q_{gg12} and Q_{gg4} peaks observed in figure 1(e), are featureless, and are not shown.

The cross-section for the ^{7}Li(^{18}O,α ^{15}N)^{6}He proton transfer reaction has been obtained from the observed yield in the ^{19}F excitation energy spectra shown in figure 5. The yields, integrated between E_x = 8–17 MeV in the 80 MeV beam data and E_x = 7.5–23 MeV in the 100 MeV beam data, were efficiency corrected following Monte Carlo simulations (described above) performed over these same excitation energy ranges. The measurement was only sensitive to the backward angle component of the ^{7}Li(^{18}O,α ^{15}N)^{6}He reaction, the centre-of-mass scattering angles covered being θ^* = 100°–160° for the 80 MeV beam data and θ^* = 95°–160° for the 100 MeV beam data. Over these ranges the cross-sections are

Table 3. Cross-sections for the various decay channels.

Channel	Beam energy (MeV)	E_x (MeV)	σ (μb)
^{7}Li(^{18}O,α ^{15}N)^{6}He	80	8.0–17.0	31.7 ± 6.6
^{7}Li(^{18}O,α ^{15}N)^{6}He	100	7.5–23.0	31.8 ± 6.6
^{7}Li(^{18}O,α ^{15}N)^{6}He	80	9.72	0.87 ± 0.23
^{7}Li(^{18}O,α ^{15}N)^{6}He	80	10.32	1.24 ± 0.30
^{7}Li(^{18}O,α ^{15}N)^{6}He	100	15.18	1.38 ± 0.37
^{16}O(^{18}O,α ^{6}He)^{24}Mg	80	9.0–20.7	<1.9
^{16}O(^{18}O,α ^{6}He)^{24}Mg	100	9.8–26.1	<3.9
^{12}C(^{18}O,α ^{6}He)^{20}Ne	80	9.0–20.7	<52
^{12}C(^{18}O,α ^{6}He)^{20}Ne	100	9.8–26.1	<65

$\sigma = (31.7 \pm 6.6)$ μb at 80 MeV and (31.8 ± 6.6) μb at 100 MeV (table 3). The quoted uncertainties are dominated by an estimated 20% error in the target thickness. Also included in table 3 are the cross-sections obtained for the individual peaks observed in figure 5. These were obtained by fitting Gaussian line shapes to the peaks above smoothly varying backgrounds. The yields were then efficiency corrected following Monte Carlo simulations at the relevant excitation energy in ^{19}F.

In order to obtain an upper limit to the cross-section for the ^{16}O(^{18}O,α ^{6}He)^{24}Mg reaction, a number of Monte Carlo simulated events were added to the total energy spectra shown in figures 1(a) and (d). In each case the number of Monte Carlo events required to produce a clearly discernible peak at the predicted Q_{ggg} peak energy was taken as the maximum possible experimental yield. The simulations were performed over the same ^{10}Be excitation energy range as is observed in figure 4, $E_x = 9.0$–20.7 MeV for the 80 MeV beam data and $E_x = 9.8$–26.1 MeV at 100 MeV. Once obtained, the yields were efficiency corrected and the cross-sections determined. The upper limits were found to be $\sigma < 1.9$ μb and <3.9 μb at 80 and 100 MeV, respectively (table 3). A similar analysis for the ^{12}C(^{18}O,α ^{6}He)^{20}Ne channel, using the same excitation energy ranges as in the ^{16}O target case noted above, resulted in values of $\sigma < 52$ μb at 80 MeV and $\sigma < 65$ μb at 100 MeV (table 3). The large difference in upper limits between these two target constituents mainly reflects the very different nominal target thicknesses of 10 μg cm^{-2} for the ^{12}C backing and $\sim$107 μg cm^{-2} for the ^{16}O content of the Li_2O foil. It is noted that although a weak peak is seen at the predicted Q_{ggg} energy for the ^{12}C(^{18}O,α ^{6}He)^{20}Ne reaction at 80 MeV (figure 1(c)), it is likely that most, if not all, of these events arise from the Q_{gg12} events seen in figure 1(b). These would appear as a broad peak in figure 1(c) due to the use of the incorrect recoil mass in the E_{tot} calculation. Using the yield in the peak observed in figure 1(c) to obtain a cross-section is therefore not reliable, and hence an upper limit, determined using the method described above, is given.

4. Discussion

A small, almost negligible, cross-section has been found for the population of states in ^{10}Be via the ^{16}O(^{18}O,α ^{6}He)^{24} Mg reaction (table 3). The main advantage of this reaction (from an experimental perspective) is the favourable Q-value (-11.60 MeV) when compared with, for example, that for the ^{12}C(^{18}O,α ^{6}He)^{20}Ne channel ($Q_3 = -13.75$ MeV). The less negative reaction Q-value would, in principle, be expected to result in a larger reaction cross-section. An additional advantage of the ^{16}O(^{18}O,α ^{6}He)^{24}Mg reaction is that it has the potential to populate a variety of states of differing single-particle structure. The removal of two α-

particles from ^{18}O could populate $2p$–$2h$ structures in ^{10}Be, where the two valence neutrons are in the sd-shell. Similarly, the removal of $2p$+α from the ^{16}O target would produce ^{10}Be states where all nucleons reside in the $1p$-shell. This is a particularly attractive feature, as is the use of a reaction in which all of the initial and final-state nuclei have ground state spin/parities of 0^+, allowing a model independent spin analysis to be performed. The question then arises as to why the cross-section for the population of such states is so low. The ^{24}Mg + ^{10}Be* final state can be reached via a number of different reaction paths. One is compound nucleus formation followed by ^{10}Be emission. Calculations using the code PACE4 [10] indicate a fusion-evaporation cross-section for this channel of $\sim$10 mb (compared to a total cross-section of $\sim$100 mb) at a beam energy of 100 MeV. The predicted cross-section is <0.1 mb at 80 MeV. It is clear in the present work that the experimental cross-section is strongly suppressed compared to these predictions, probably for structural reasons. An alternative population mechanism is direct transfer. Calculations of the optimum angular momentum transfer in this reaction, based on the change in centre-of-mass energy and the associated change in orbital angular momentum between the entrance and exit channels, suggest that the optimum angular momentum transfer is 7–9$\hbar$ for ^{10}Be excitation energies of 9–15 MeV (at both beam energies). It is possible that the poor angular momentum matching between the states of lower spin in ^{10}Be resulted in the observed small reaction cross-section. In this respect the use of a ^{12}C target is no better. However, as shown in the work of Bohlen *et al* [4], the two-proton stripping reaction ^{12}C(^{12}C,^{14}O)^{10}Be* does populate ^{10}Be excited states, but has a very negative Q-value (-20.6 MeV) and is not well suited to the present technique due to the expected backward angle emission of the ^{10}Be nucleus. The ^{12}C(^{14}C,^{10}Be*) reaction ($Q = -4.85$ MeV) is a possible alternative, which will be explored in the near future.

Breakup studies of reactions such as ^{7}Li(^{18}O,α ^{15}N)^{6}He typically populate states that have large widths for the cluster partition (α + ^{15}N in this case). It might be expected, therefore, that the subset of ^{19}F states observed in figure 5 may be associated with an α-cluster structure. The ^{7}Li(^{18}O,^{19}F)^{6}He reaction involves the transfer of a proton from the ^{7}Li target to the ^{18}O projectile. This transfer could proceed to the sd-shell, populating cluster states above the α-decay threshold at 4.01 MeV. States populated in this manner would naturally be expected to have a t + ^{16}O type cluster structure, and be possible analogues of the well-known α + ^{16}O clusters states in ^{20}Ne [11, 12]. States which strongly α-decay would require a $1p$–$1h$ excitation of the ^{16}O core, with a proton being excited to the sd-shell. Such states would be described in terms of a α + ^{15}N cluster partition. This would be an alternative analogue to the α + ^{16}O cluster structure in ^{20}Ne, where a proton is removed from the ^{16}O core (to give α + ^{15}N) rather than from the α-particle (producing t + ^{16}O). In the present ^{7}Li(^{18}O,^{19}F)^{6}He reaction the population of such states would rely on a two-step process: the inelastic excitation of the ^{18}O projectile followed by transfer. In this experiment the ^{19}F nuclei were observed to be emitted at backward centre-of-mass angles where such complex two-step processes are more favoured. In the context of the above discussion it would be interesting to study the t + ^{16}O decay of ^{19}F at forward angles in order to better understand the competition between the t + ^{16}O and α + ^{15}N cluster partitions. It was not possible to observe this decay channel in the present measurements.

5. Summary and conclusions

A search has been made for the α + ^{6}He decay of ^{10}Be via the ^{16}O(^{18}O,α ^{6}He)^{24}Mg reaction. No evidence was obtained for such a decay, the cross-section being $\sigma < 1.9$ μb at a beam energy of 80 MeV and <3.9 μb at a beam energy of 100 MeV. The α + ^{15}N decay of ^{19}F was seen via the ^{7}Li(^{18}O,α ^{15}N)^{6}He reaction and a number of peaks observed in the ^{19}F excitation

energy spectra. Other than the peak observed at 15.18 MeV, which may be associated with the 14.72 or 14.74 MeV states in ^{19}F, it has not been possible to associate the peaks with known states. The cross-section for this channel is $\sigma = (31.7 \pm 6.6)$ and (31.8 ± 6.6) μb at 80 and 100 MeV, respectively.

Acknowledgments

The assistance of the staff at the Australian National University (ANU) 14UD tandem facility is gratefully acknowledged. This work was funded by the United Kingdom Science and Technology Facilities Council (STFC). The experimental work was performed under a formal agreement between the STFC and ANU.

References

[1] Hamada S, Yasue M, Kubono S, Tanaka M H and Peterson R J 1994 *Phys. Rev.* C **49** 3192–99
[2] Curtis N, Ashwood N I, Clarke N M, Freer M, Metelko C J, Soić N, Catford W N, Mahboub D, Pain S and Weisser D C 2004 *Phys. Rev.* C **70** 014305
[3] Freer M 1996 *Nucl. Instrum. Methods* A **383** 463–72
[4] Bohlen H G, Dorsch T, Kokalova Tz, von Oertzen W, Schulz Ch and Wheldon C 2007 *Phys. Rev.* C **75** 054604
[5] Soić N *et al* 1996 *Europhys. Lett. 1* **34** 7–12
[6] Curtis N, Caussyn D D, Fletcher N R, Maréchal F and Fay Nand Robson D 2001 *Phys. Rev.* C **64** 044604
[7] Freer M *et al* 2006 *Phys. Rev. Lett.* **96** 042501
[8] Tilley D R, Kelley J H, Godwin J L, Millener D J, Purcell J E, Sheu C G and Weller H R 2004 *Nucl. Phys.* A **745** 155–362
[9] Tilley D R, Weller H R, Cheves C M and Chasteler R M 1995 *Nucl. Phys.* A **595** 1–170
[10] Gavron A, Hillman M and Eyal Y computer code PACE (unpublished)
[11] Bromley D A 1985 *Proc. of the 4th Int. Conf. on Clustering Aspects of Nuclear Structure and Nuclear Reactions (Chester, UK)* ed J S Lilley and M A Nagarajan (Dordrecht: Reidel) p 1
[12] Tomoda T and Arima A 1978 *Nucl. Phys.* A **303** 217–53